Design concept for an aluminium valve body under high internal cyclic pressure loading based on autofrettage; design rule for autofrettage pressure based on static non-linear finite element simulations and experimental verification

Stephan Sellen[a*], Stefan Maas[a], Thomas Andreas[b], Peter Plapper[a], Arno Zürbes[c], Daniel Becker[b]

[a] University of Luxembourg, Campus Kirchberg, L-1359, Luxembourg
[b] Rotarex S.A., Lintgen, L-7440, Luxembourg
[c] FH-Bingen, D-55411, Germany

Abstract

The following paper is intended to improve the fatigue behaviour of a complex aluminium valve geometry under high internal cyclic pressure loading. The autofrettage process helps to increase the fatigue durability and a simple but efficient design method for this process is pointed out. Based on non-linear material's behaviour, finite element simulations of the crack-free geometry help to determine the minimum and maximum autofrettage pressure to be used, without iterative crack simulations, which would require a lot of computational time. Material tests under inverse plastifications were performed in order to determine the correct material model. The derived design method was verified with simplified specimens subjected to different autofrettage pressure levels and subsequent cyclic fatigue tests.

Keywords

Fracture, aluminium, autofrettage, residual compressive stress, lightweight design, non-linear finite element simulation.

*Corresponding author: sellen.stephan@rotarex.com; Phone: +352 32 78 32-608

Content

1 Introduction

The requirement of lightweight design for continuously higher pressure of gases leads to the use of aluminium for valve bodies, which hence have to withstand fluctuating high pressure. Figure 1 shows the example of a hand-sized aluminium valve body, whose mechanical design is discussed subsequently.

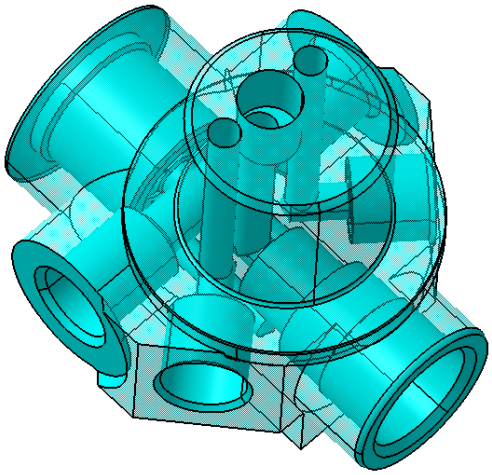

Figure 1: Typical design of a valve body of an on-tank valve for gaseous applications

Many bore intersections in this aluminium valve body cause high stress concentrations due to the internal pressure. According to the testing guideline [1], the valve has to withstand a maximum static test pressure of 105 MPa and a cyclic hydraulic pressure test of N=150,000 cycles with a cyclic pressure loading of 87.5 MPa (stress ratio value $R = 0$). The first experiments were done with simplified test bodies of aluminium AW-6082-T6 and are shown in Figure 2.

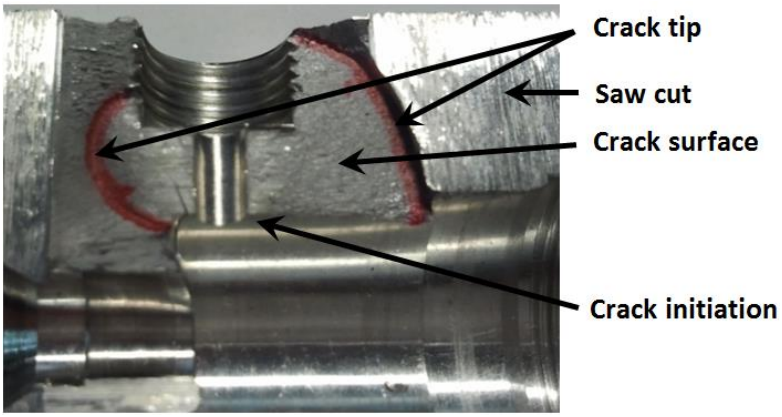

Figure 2: Simplified test specimen opened after cyclic pressure testing

After less than 100,000 cycles with a pressure range of 0-87.5 MPa ($R = 0$), deep cracks occurred, starting from the rectangular bore intersection and leading to high stress concentration, i.e. the design target was largely missed (Figure 2).

To overcome this difficulty, the process of autofrettage was applied to this aluminium part. In the end, with a correct design, far more than 150,000 pressure cycles became possible using a correct autofrettage pressure.

2 State of the art

While using the autofrettage process, a very high static autofrettage pressure of several hundred MPa is applied once to the inner tube. The critical inner layer with locally high circumferential stresses on the thick-walled tube is plastically deformed. While discharging to $p_i = 0$, these plastically deformed parts are set under residual compressive stress by the outer layers of the tube, which were only elastically charged. In Figure 3, on the left we see the elastic stress distribution in the tube shell during the application of internal pressure. When the autofrettage pressure is applied and later released, this inner point is strained above the yielding point. It is later shifted into the compression zone by the outer zones of the tube, which are only elastically stressed due to the steep stress gradient, which can be seen on the left. σ_m and σ_a are an example for a permitted stress mean and amplitude value without autofrettage, whereas $\sigma_{m,af}$ and $\sigma_{a,af}$ symbolize the same permitted stress values after autofrettage. The permitted amplitude is dependent on the mean value σ_m, which can also be seen in the HAIGH-diagram on the right, which shows the endurance limits as a function of the mean stress σ_m.

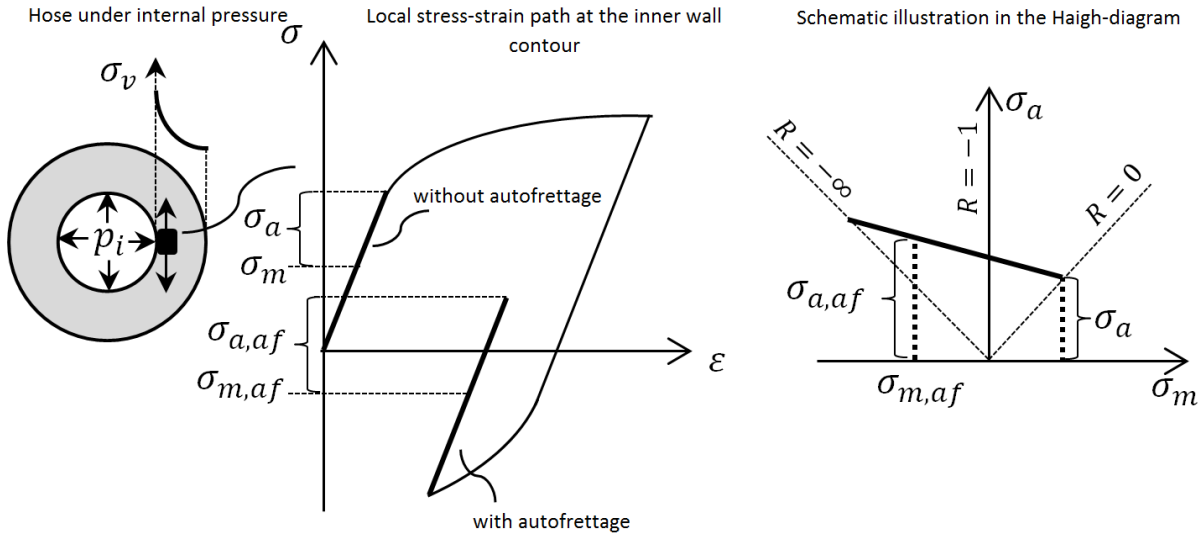

Figure 3: Autofrettage effect related to fatigue mechanics for an internally pressurized thick-walled hose, related to [12]

Hence autofrettage in our case can be used to shift the mean stress from $\sigma_m = \sigma_a(R = 0)$ to negative values. This technique does not only work for a plain thick-walled tube, but also for complex intersecting bores in a valve body.

A considerable amount of work had been accomplished towards the autofrettage process and the optimum choice of the autofrettage pressure level for simple thick-walled steel cylinders as well as investigations on the increased fatigue life and the crack growth in the residual stress zones under mechanical loads [2, 3, 4…, 12].

Greuling [13] studied the crack growth behaviour of internally pressurized bore intersections of tubes under an intersection angle of 90° and 45° respectively for stainless steel (42CrMo4) with the help of fracture mechanics near the fatigue limit. The estimation of the crack growth was done by weight functions. However, a transfer to complex geometries was not done and is not evident. Lechmann [14] used numerical crack growth simulation tools in order to estimate the crack growth in a three-dimensional steel structure with one bore intersection of tubes. But this numerical procedure requires a lot of computational time for a complete valve body with several bore edges.

Hence the following questions arise:

- What is the minimum, the optimum and the maximum autofrettage pressure?
- How can the initial crack length after autofrettage and its growth due to cyclic loading be assessed?
- Which non-linear material model can describe the inverse plastification behaviour of aluminium?

2.1 CONSIDERATION OF RESIDUAL COMPRESSIVE STRESSES

There are some approaches to combine the effect of residual compressive stresses with the linear elastic fracture mechanics (LEFM).

The FKM-guideline "Bruchmechanischer Festigkeitsnachweis für Maschinenbauteile" [15] suggests to add residual stresses to the maximum and minimum load stresses:

$$\Delta K = K\left(\sigma_{max} + \sigma_{eig}\right) - K\left(\sigma_{min} + \sigma_{eig}\right) \tag{1}$$

This means that the cyclic stress intensity factor range ΔK remains constant and the ratio R_K =K_{min}/K_{max} of the intensity factor is shifted. But on the other hand, a crack can only grow if it is opened during the cycle. Thus, if the maximum stress intensity factor theoretically is still negative due to the residual stress, the crack cannot open.

In case of internally pressurized tubes, a fracture mode-I is responsible for a possible crack growth [14]. As an example, the cyclic stress intensity factor ΔK is often calculated for simple geometrical models (e.g. a plane with a side crack) using the cyclic stress range and a correction factor Y_I depending on the geometry and the crack length a (Figure 4):

$$\Delta K = \Delta\sigma \cdot \sqrt{\pi \cdot a} \cdot Y_I(a, d) \tag{2}$$

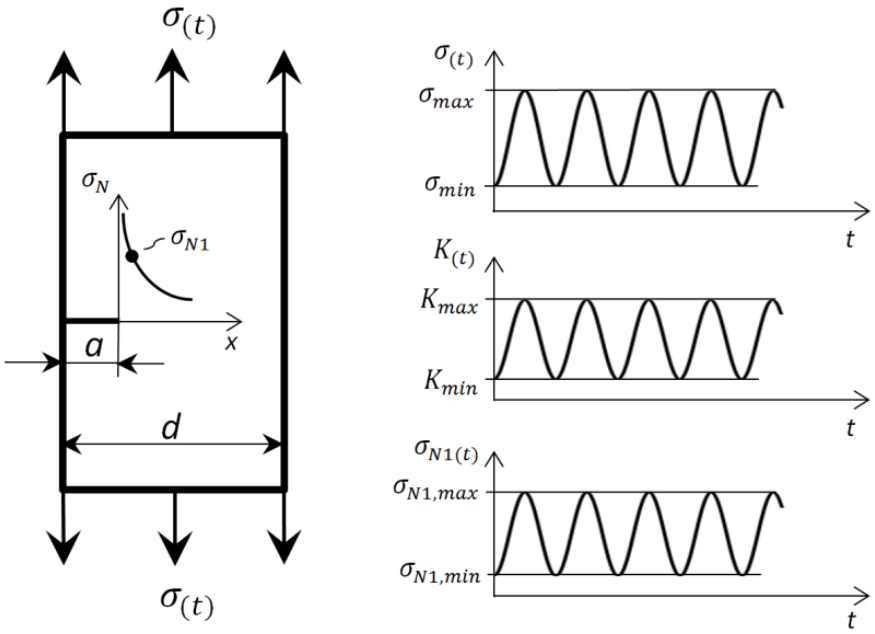

Figure 4: Side crack in a plane geometry with the load σ(t) causing a fracture mode-I, refer to Richard and Sander [23]

The maximum and minimum of K are calculated as follows

$$K_{max} = \sigma_{max} \cdot \sqrt{\pi \cdot a} \cdot Y_I(a, d) \tag{3}$$

and

$$K_{min} = \sigma_{min} \cdot \sqrt{\pi \cdot a} \cdot Y_I(a, d) \tag{4}$$

This approach is no longer feasible in case of complex geometries as the geometrical factors Y_I are no longer known; therefore another simplified approach is subsequently proposed.

3 A calculation method for complex geometries based on fracture mechanics

The initial plastification caused by the autofrettage pressure (load step 1 (LS 1)) and the subsequent inverse plastification due to the load relieve (LS 2) are generally followed by a cyclic elastic normal stress range due to internal pressure cycles (minimum normal stress: LS 2,4,6,8,…; maximum normal stress: LS 3,5,7…see Figure 5).

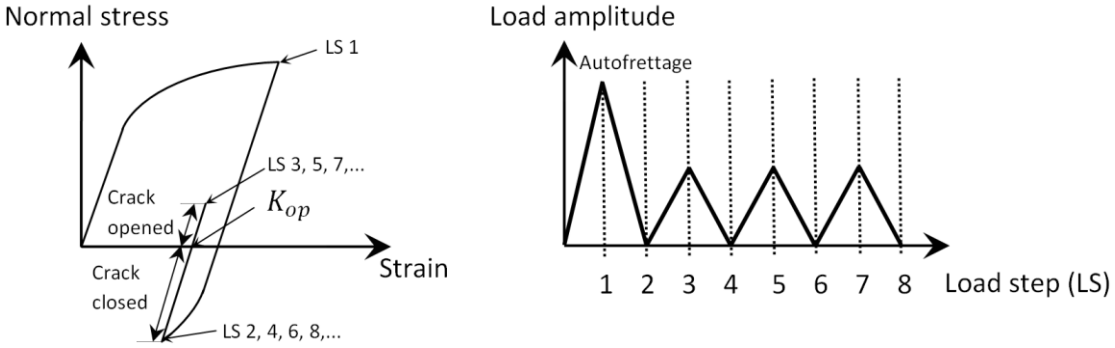

Figure 5: Cyclic range of normal stresses under autofrettage and subsequent cyclic load test

Under the assumption that only autofrettage induces plastification and the subsequent cyclic range of the normal stress behaves elastically, one may neglect a small plastic zone at the crack tip (this justifies the application of the linear elastic fracture mechanics LEFM). The crack only opens if the maximum tensile stresses are positive (Figure 5).

The effective cyclic stress intensity factor range ΔK_{eff} describes the difference between the maximum stress intensity factor K_{max} and the minimum stress intensity factor for crack opening K_{op} [16, 17]. The effective range for the cyclic stress intensity factor ΔK_{eff} is thus

$$\Delta K_{eff} = \begin{cases} K_{max} - K_{min} & for\ K_{max} > 0\ and\ K_{min} > 0 \\ K_{max} - K_{op} = K_{max} & for\ K_{max} > 0\ and\ K_{min} \leq 0 \\ 0 & for\ K_{max} \leq 0\ and\ K_{min} < 0 \end{cases} \quad (5)$$

Furthermore, if the crack length a is constant, i.e. the crack does not grow, the load stress ratio R_σ for any cyclic loading can be set equal to the stress intensity ratio R_K due to the elastic behaviour and the assumptions of the linear elastic fracture mechanics (LEFM, equations (2), (3) and (4), Figure 4):

$$R_\sigma = \frac{\sigma_{min}}{\sigma_{max}} = R_K = \frac{K_{min}}{K_{max}} = R_{\sigma N} = \frac{\sigma_{N,min}}{\sigma_{N,max}} \quad (6)$$

For a cyclic normal stress range leading to a cyclic stress intensity range under a mode-I loading with autofrettage and subsequent elastic behaviour, both ranges are again proportional, i.e. equations (2), (3) and (4) are still valid:

$$\Delta\sigma_N = k \cdot \Delta K_I \quad (7)$$

It should be noted that autofrettage normally causes locally non-linear material deformation, which is subsequently followed by an elastic cyclic stress range (LS 3, 4, 5…).

3.1 CONSIDERATION OF THE THRESHOLD STRESS INTENSITY FACTOR

The distinction if a crack is growing or not under cyclic loading is defined by the cyclic threshold stress intensity range ΔK_{th}, which is somewhat dependent on the stress intensity ratio R [18]. A long crack (macroscopic crack) is not growing if (Figure 6):

$$\Delta K_{eff} < \Delta K_{th}(R) \tag{8}$$

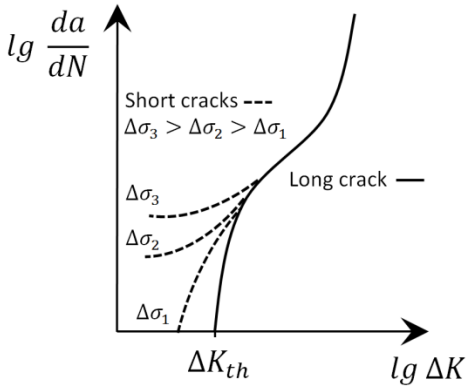

Figure 6: Schematic illustration of a crack growth curve, referring to Radaj [26]

Despite the shown threshold behaviour for a long crack under the prerequisites of the LEFM, short cracks (or micro-cracks) can grow even below that theoretical limit.

3.2 SIMPLIFIED METHOD FOR COMPLEX GEOMETRIES

Because of the stated uncertainties for the exact determination of the cyclic stress intensity threshold ΔK_{th}, a conservative approach according to the third line of equation (5) can be done: For any crack length, the condition $\Delta K_{eff} = 0 \leq \Delta K_{th}$ is complied with if the maximum stress intensity factor is always

$$K_{max} \leq 0 \tag{9}$$

which is true according to equation (3) if the relevant normal stress is always

$$\sigma_{N,LS3} \leq 0 \tag{10}$$

Under these conditions (equation (9), (10)) no crack can grow as always $\Delta K_{eff} \leq \Delta K_{th}$ (except mirco-cracking) and the problem can be merely reduced to an elastic-plastic finite element simulation of the crack-free geometry for the first three load steps, without the need to simulate different cracks and depths at different locations in order to determine the cyclic stress intensity factor ranges, i.e. no incremental and iterative crack growth simulations. For a complex valve body, this leads to large computational time savings.

The proposed procedure may be summarized as follows:

1. Linear-elastic finite element simulation of the whole structure (e.g. with a unit pressure of 1 MPa)
    - Localisation of the critical points or notches to be considered
    - If necessary, refining of the mesh at these points and determination of the elastic equivalent stresses at these notches

- Derivation of the crack plane orientation normal to the first principal stress σ_1 at this notch

2. Estimation of the maximum autofrettage pressure by an iterative approach

- Criterion: The maximum autofrettage pressure should cause a strain level at the critical notch somewhat below the material's fracture strain

3. Elastic-plastic finite element simulation for the first three load steps (LS 1-LS 3) and evaluation of the stress perpendicular to the potential identified crack plane. In the following, this stress is simply denominated "normal stress".

- Evaluation of the normal stress perpendicular to the above predefined crack plane orientation for load step 1 under autofrettage pressure
- Evaluation of the normal stress perpendicular to the above predefined crack plane orientation for load step 2 by complete pressure relief
- Evaluation of the normal stress perpendicular to the above predefined crack plane orientation for load step 3 under maximum operating pressure
- Plot of the normal stress distribution of load step 3 in the crack plane at the tip of the notch (volume under compressive stress)
- Review of the volume: It should have a reasonable size with a thickness clearly exceeding the surface roughness, i.e. it should penetrate into the body some millimetres from the surface. Possible adaption of the autofrettage pressure and repeat calculation of load steps LS 1 to LS 3. If the autofrettage pressure was too high compared to the defined criterion of not exceeding the material's fracture strain, the pre-induced crack length has to be estimated.

4 Verification of the method

To verify the proposed approach, a simplified test geometry was defined. The normal stresses in the estimated crack plane were calculated for the first three load steps using non-linear elastic-plastic finite element simulations. To specify the non-linear material behaviour exactly, specimens were machined for tensile and subsequent compressive tests.

4.1 NON-LINEAR MATERIAL BEHAVIOUR OF ALUMINIUM AW-6082-T6

In order to calculate the residual compressive stresses after autofrettage, the hardening effect of the material has to be taken into account. Static tensile tests were conducted to a predefined strain level of 2%, 4%, 6% and 8% with subsequent load reversal. All curves showed the same stress-strain behaviour as the illustrated example of 2% maximum strain (Figure 7).

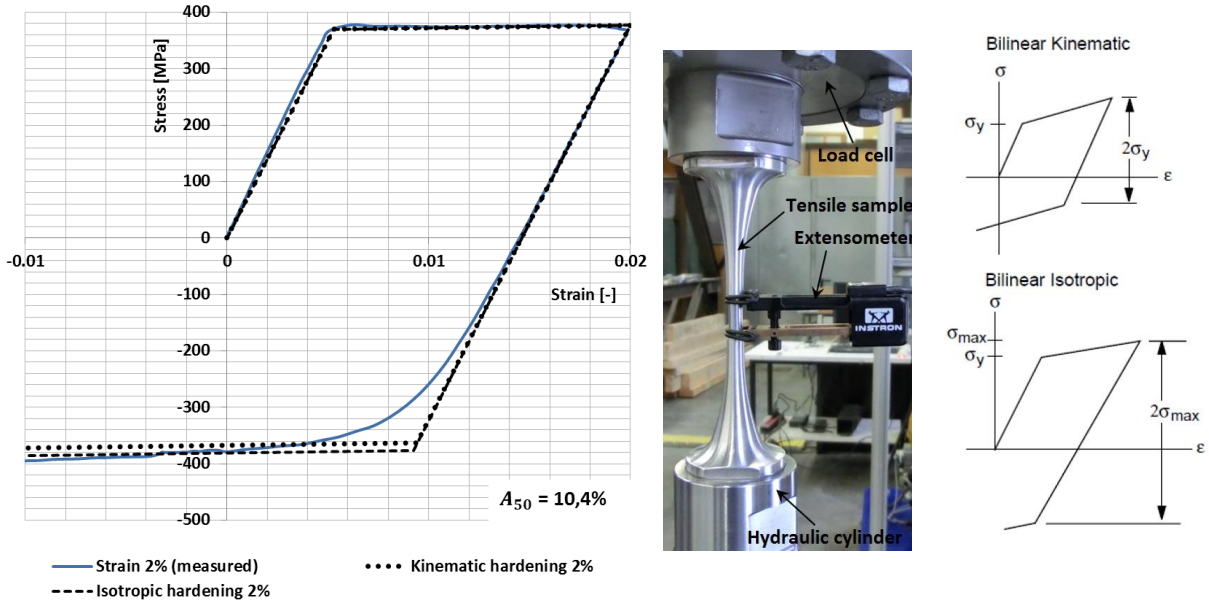

Figure 7: Static material stress-strain-curve with aluminium specimen: pull and push, strain controlled (here ε ≤ 2%). Idealized material models for isotropic and kinematic hardening according to ANSYS [27] are indicated.

The tests show nearly bilinear stress-strain behaviour. It can be seen that the radius of the inverse plastification is different from the Masing approach [21] and the reverse radius is more than 2 times the radius of the first plastification. For the strain curve ending at 2%, the idealized models of bilinear isotropic and of kinematic hardening were included with dotted lines. The kinematic hardening model is more conservative as there is a direction-dependent change of the material's proportional limit after a primary plastic deformation, which is also known as the Bauschinger effect [22]. As the assumption of the bilinear kinematic hardening model shows a good accordance with the tests, it was used as material model for the finite element simulations, respecting the von Mises yield criterion and the associative flow rule [20]. Thus only by definition of the yield strength (here $R_p = \sigma_y = 371\ MPa$), the modulus of elasticity (here $E = 76{,}500\ MPa$) and the tangent modulus (here $T = 843\ MPa$), can the material's behaviour be described. It is important to note that for the used aluminium alloy a fracture strain of $A_g = 10.4\ \%$ was measured.

4.2 DEFINITION OF SIMPLIFIED TEST GEOMETRY

Figure 8 shows the simplified aluminium test geometry with a 90° bore intersection with different bore diameters.

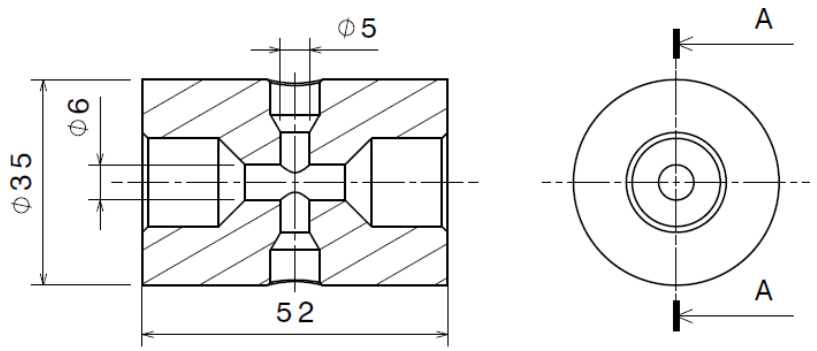

Figure 8: Geometry of the simplified test specimen (material: AW-6082-T6)

During the autofrettage procedure and the subsequent cyclic testing, screwed end plugs were used, which tightened at the metallic cones.

4.3 SIMULATION AND EXPERIMENTAL RESULTS

As mentioned above for the simplified method for aluminium, the normal stress at the third load step LS3 needs to be negative. In the following, the normal stress distribution rectangular to the crack plane at the tip of the notch for the third load step as a result of the elastic-plastic finite element simulation and also the experimental results are presented.

4.3.1 SIMULATION MODEL

For the simulation with ANSYS, which is based on symmetry, only one eighth was necessary. The element type SOLID187 was chosen to generate the mesh, which was locally refined at the tip of the bore intersection, where the highest stress concentration occurs (Figure 9):

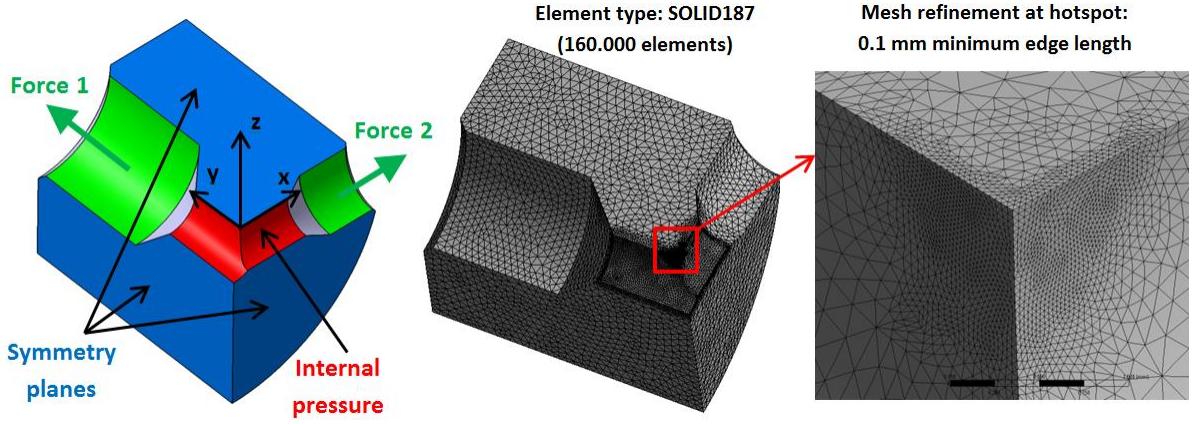

Figure 9: Simulation model, applied loads and meshing

The three important load steps (autofrettage pressure (LS 1), complete relief (LS 2) and maximum operating pressure (LS 3)) of the crack-free geometry were simulated, including the pressure forces of the plugged ends. For the evaluation of the occurring stresses at the tip of the bore intersection, a local coordinate system was defined (Figure 9). The non-linear material model was derived from the

above mentioned tests, while the measured static stress strain curve (σ_{ing}, ε_{ing}) of the tensile specimen was converted to a logarithmic strain ε_{log} and a real stress σ_{real}. This conversion helps to correct the effect of specimen elongation and of area reduction in the tensile test and thus leads to the true or real values. It is based on the following equations, which are recommended by Rust [23]:

$$\varepsilon_{log} = ln(1 + \varepsilon_{ing}) \tag{11}$$

$$\sigma_{real} = \sigma_{ing}(1 + \varepsilon_{ing}) \tag{12}$$

4.3.2 *INITIAL CONDITION*

During a hydraulic cyclic pressure test at room temperature, the test body failed after 156,000 cycles ($\Delta p = 0 - 87.5\ MPa,\ i.e. R = 0$) at the metallic tightening cone due to large cracks. After testing, the specimen was saw cut, clearly showing the crack (Figure 10).

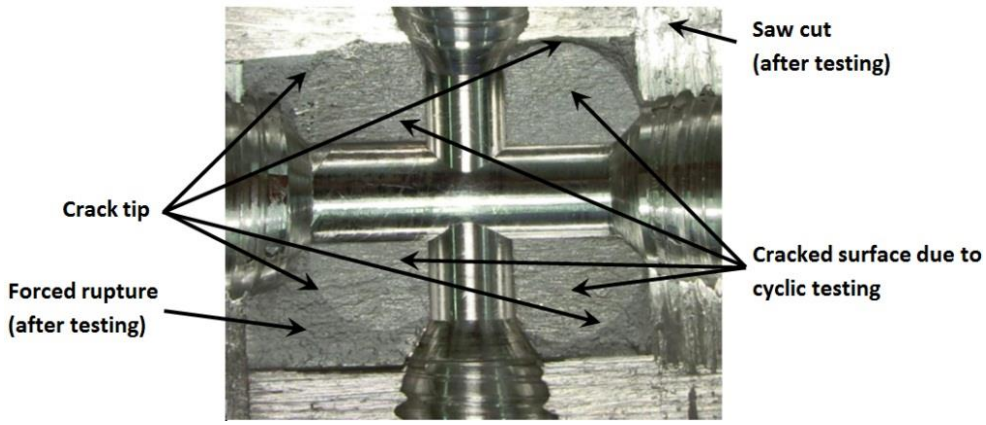

Figure 10: Tested specimen without autofrettage after N=156,000

All four edges show a similar crack shape with almost the same crack length.

4.3.3 *AUTOFRETTAGE WITH A PRESSURE OF 180 MPA*

After autofrettage with a pressure of 180 MPa, the normal stress σ_N distribution perpendicular to the potential crack plane within the local coordinates x and y for the maximum operating pressure (LS 3) was calculated in a non-linear finite element calculation by using the material law of equation (11) and (12) respectively. It shows just a small volume at the tip, where the stresses are negative (Figure 11).

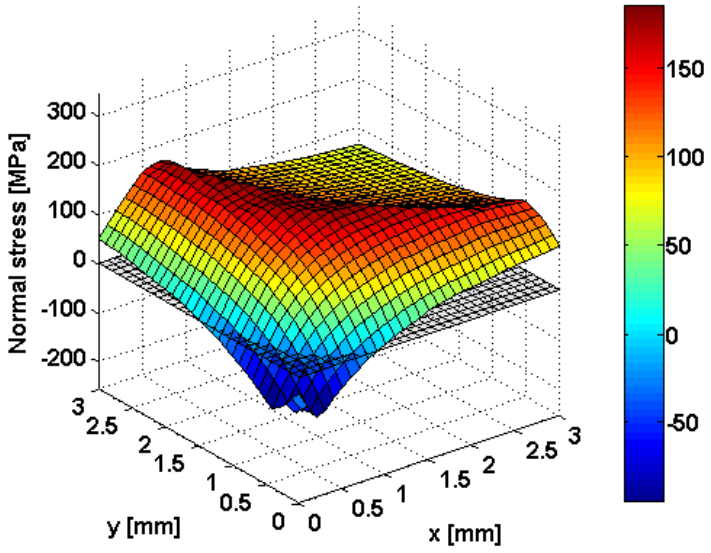

Figure 11: Normal stress distribution at the notch under maximum operating pressure (LS3) after autofrettage with 180 MPa

The compression zone is very small with a depth of about 0.2-0.6 mm and hence the crack can start nearby. Additionally, with respect to the surface roughness, it is clear that this volume is too small to avoid crack growth.

The experiment shows interesting results with partly irregular crack growth at the four notches of the two specimens (Figure 12). This irregularity makes us presume that the cyclic stress intensity factor range ΔK_{eff} is close to the threshold value for crack growth. However, it should be noted that the number of cycles prior to complete failure could already be increased to 368,000 cycles.

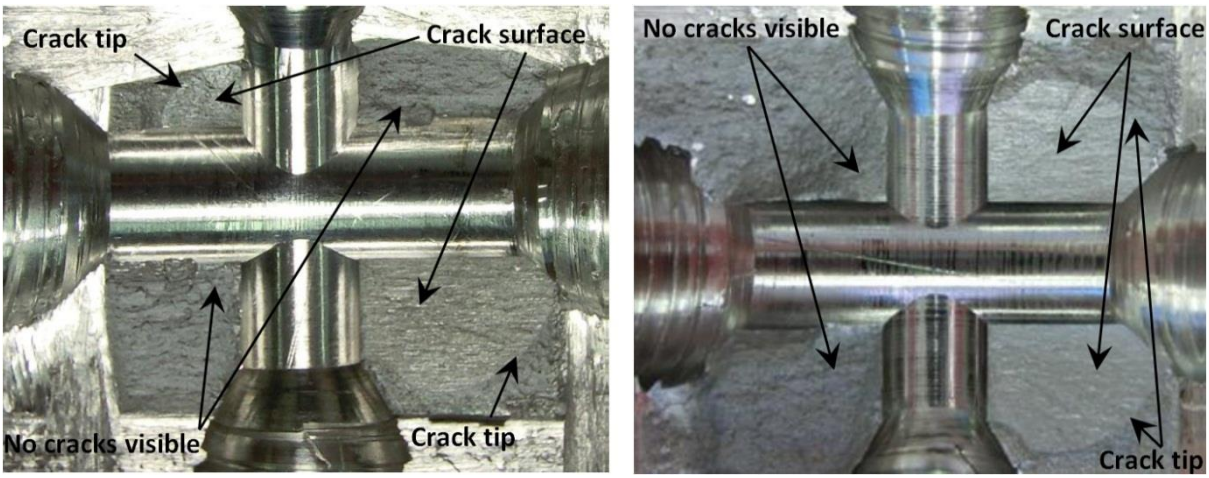

Figure 12: Two opened test bodies after cyclic testing (368,000 cycles, autofrettage pressure: 180 MPa)

4.3.4 AUTOFRETTAGE WITH A PRESSURE OF 270 MPA

With an increased autofrettage pressure, the volume under compression in LS3 is significantly larger, while the thickness of this layer is more than 1 mm at the notch and reaches 0.3 to 0.5 mm in the bores (Figure 13).

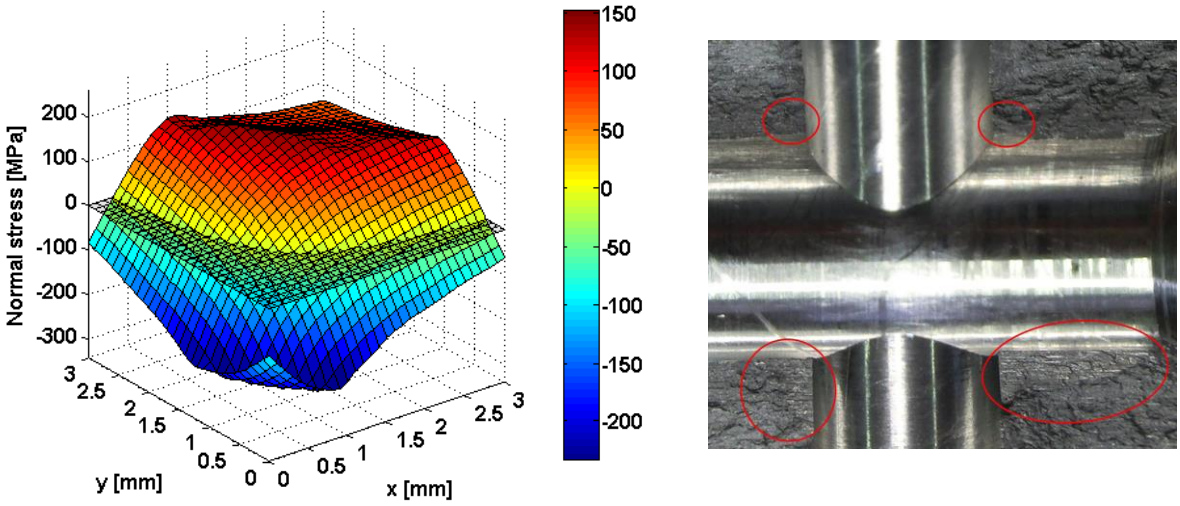

Figure 13: Normal stress distribution at the intersection notch after autofrettage with 270 MPa and subsequent application of maximum operating pressure (LS3) (left); opened specimen after 10^6 cycles (right)

In Figure 14, the relevant stress range $\Delta\sigma_N$ is shown; it is interesting to note, that this range quickly decreases from 250 MPa to values around 50 MPa when we are going from the surface into the body.

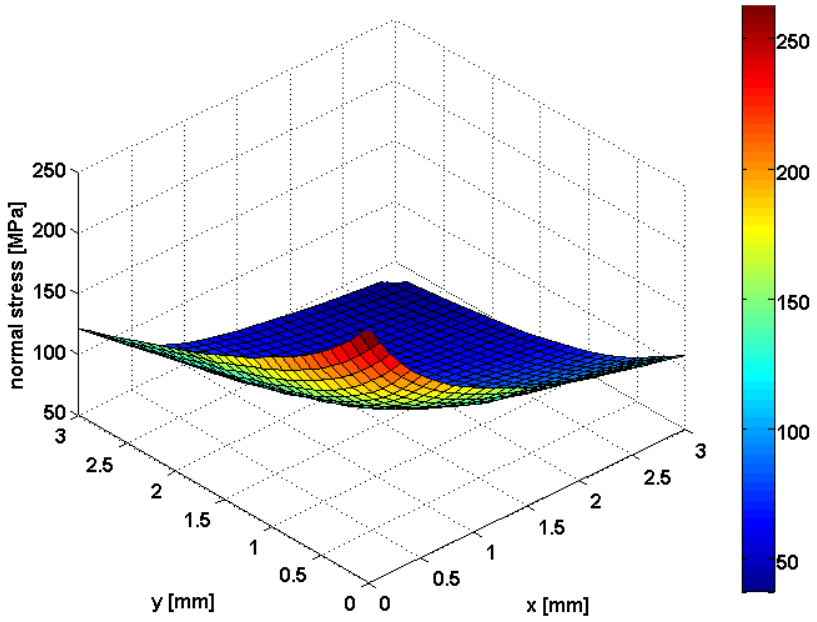

Figure 14: Normal stress range (LS2 to LS3) at the intersection notch due to the cyclic pressure loading

This effect can also be seen in the experimental results as, after 10^6 cycles, the specimen showed only very small cracks.

4.3.5 AUTOFRETTAGE WITH A PRESSURE OF 350 MPA

Another fatigue test was performed with a specimen after autofrettage with 350 MPa, with a maximum total equivalent strain of about 5% at the notch. As the materials' fracture strain A_g is more than 10 %, no initial crack is introduced during the autofrettage and, even after 1 million cycles, only small fatigue cracking occurred (Figure 15).

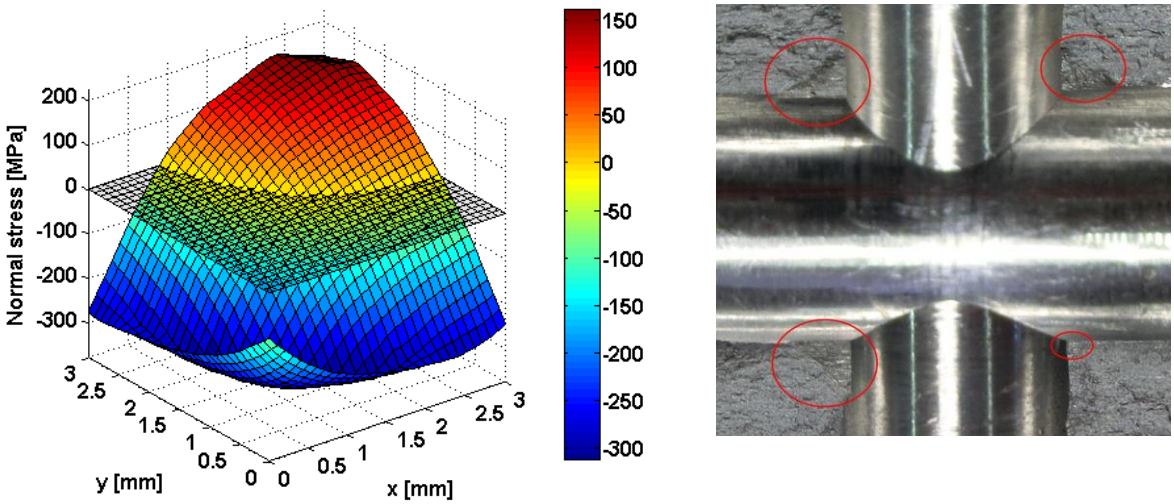

Figure 15: Normal stress distribution at the intersection notch after autofrettage with 350 MPa and subsequent application of maximum operating pressure (LS3) (left); opened specimen after 10^6 cycles (right)

The simulation shows a reasonable volume under compression even in the third load step (LS3) with a depth between 1 mm and 2 mm. This test was also stopped after 10^6 cycles and the sample opened and, just the same as with the autofrettage pressure of 270 MPa, only small cracks became visible.

5 Results and Conclusion

Tests with simplified aluminium specimens under an internal cyclic pressure showed quick crack growth. This behaviour changed after autofrettage and significantly improved durability was shown. The specimens reached 10^6 cycles with only very small cracks. Hence, in the case of aluminium, autofrettage shows an interesting potential.

To determine the maximum autofrettage pressure at the critical notch, a criterion "strain level somewhat below the material's fracture strain" during autofrettage was used within a non-linear finite element analysis, applying a conservative kinematic hardening materials' model with only three parameters. No pre-existing defects or cracks were modelled. The minimum autofrettage pressure should be such that a reasonable volume with a thickness of some millimetres is under compression in the potential crack plane. The stress range should respect the materials' fatigue limit for $R = -\infty$ according to the HAIGH diagram. The above described method was successfully applied to aluminium test specimens and more than 1 Million cycles were also reached with $\Delta p = 0 - 87.5\ MPa, i.e. R = 0$.

6 Outlook

The small induced cracks at the tip after 1 million cycles are currently under investigation with different fatigue design methods. We also try to define the above mentioned “reasonable volume with a thickness of some millimetres under compression” more precisely. Finally, the micro-crack growth under residual compressive stresses and the residual stress relaxation has to be studied in more detail.

A complex aluminium valve for hydrogen applications was designed with these rules and several test bodies (> 10) showed promising results.

7 References

[1] Verordnung (EG) Nr. 79/2009 des Europäischen Parlaments und des Rates: Über die Typengenehmigung von wasserstoffbetriebenen Kraftfahrzeugen und zur Änderung der Richtlinie 2007/46/EG.
Amtsblatt der Europäischen Union, 14. Januar 2007

[2] Kargarnovin, M., Darijani, H. and Naghdabadi, R. (2007) Evaluation of the optimum pre-stressing pressure and wall thickness determination of thick-walled spherical vessels under internal pressure. *Journal of the Franklin Institute*, 344, 439-451.

[3] Rees, D. (2004) Autofrettage of thick-walled pipe bends. *International Journal of Mechanical Sciences*, 46, 1675-1696.

[4] Darijani, H., Kargarnovin, M. and Naghdabadi, R. (2009) Design of thick-walled cylindrical vessels under internal pressure based on elasto-plastic approach. *Materials and Design*, 30, 3537-3544.

[5] Jahed, H., Farshi F. and Hosseini M. (2006) Fatigue life prediction of autofrettage tubes using actual material behavior. *International Journal of Pressure Vessels and Piping*, 83, 749-755.

[6] Alegre J., Bravo P. and Preciado, M. (2007) Fatigue behaviour of an autofrettaged high-pressure vessel for the food industry. *Engineering Failure Analysis*, 14, 396-407.

[7] Majzoobi, G., Farrahi G. and Mahmoudi, A. (2003) A finite element simulation and experimental study of autofrettage for strain hardened thick-walled cylinders. *Materials Science and Engineering*, A359, 326-331.

[8] Zhu, R. and Yang, J. (1998) Autofrettage of thick cylinders. *International Journal of Pressure Vessels and Piping*, 75, 443-446.

[9] Maleki, M., Farrahi, G., Jahromi, B. and Hosseinian, E. (2010) Residual stress analysis of autofrettaged thick-walled spherical pressure vessel. *International Journal of Pressure Vessels and Piping*, 87, 396-401.

[10] Hojjati, M. and Hassani, A. (2007) Theoretical and finite-element modeling of autofrettage process in strain-hardening thick-walled cylinders. *International Journal of Pressure Vessels and Piping*, 84, 310-319.

[11] Schön, M., Seeger, T., Bergmann, J. W. and Vormwald, M. (1993) Autofrettage I. Forschungsvereinigung Verbrennungskraftmaschinen e.V., Frankfurt am Main.

[12] Seeger, T., Greuling, S. and Bergmann, J.W. (2001) Autofrettage II, Dauerfestigkeitssteigerung durch Autofrettage II. Forschungsvereinigung Verbrennungskraftmaschinen e.V., Frankfurt am Main.

[13] Greuling, S. (2005) Dauerfestigkeitsberechnung autofrettierter innendruckbelasteter Bauteile mit Bohrungskreuzungen unter Berücksichtigung stehen bleibender Risse. Dissertation, TU Darmstadt.

[14] Lechmann, M. (2007) Entwicklung eines schwingbruchmechanischen Konzeptes für innendruckbeanspruchte Bauteile mit ausgeprägten Druckeigenspannungsfeldern. Materialprüfungsanstalt Universität Stuttgart.

[15] Berger, C., Blauel, J.G., Hodulak, L., Pyttel, B., Varfolomeyev, I. and Gerdes, C.P. (2009) Bruchmechanischer Festigkeitsnachweis für Maschinenbauteile. VDMA Verlag, 3. edition.

[16] Richard, H.A., Sander, M. (2009) Ermüdungsrisse. Vieweg + Teubner Verlag, 1. edition.

[17] Parker, A.P. (1984) An overview of the mechanics of fracture and fatigue in the presence of residual stress. *Journal of Mechanical Working Technology*, 10, 165-174.

[18] Döker, H. (2002) Schwellenwert für Ermüdungsrissausbreitung: Bestimmung und Anwendung. In: DVM-Bericht, 234, 9-18, deutscher Verband für Materialforschung und –prüfung e. V., Berlin.

[19] Radaj. D. (2003) Ermüdungsrisse. Grundlagen für Leichtbau, Maschinen- und Stahlbau. Springer Verlag, 2. Edition.

[20] ANSYS Inc., Theory Manual: Rate independent plasticity, associated flow rule, bilinear kinematic hardening.

[21] Masing, G. (1926) Eigenspannungen und Verfestigung beim Messing. *Proc. of the 2nd Int. Congress of Applied mechanics*, 332-335.

[22] Bauschinger, J. (1886) Über die Veränderung der Elastizitätsgrenze und der Festigkeit des Eisens und Stahls durch Strecken und Quetschen, durch Erwärmen und Abkühlen und durch oftmals wiederholte Beanspruchung. Mitt. Mech.-Techn. Lab. K. Techn. Hochsch. München, 13, 108-112.

[23] Rust, W. (2011) Nichtlineare Finite-Elemente-Berechnungen. Vieweg + Teubner Verlag, 2. Edition.